Study on Hadronuclear Origin of Fermi Bubbles

Michelle Miller

September 15, 2018

INDIANA UNIVERSITY

1 Abstract

Fermi bubbles, which the Fermi Large Area Telescopes recently discovered in 2010, are two large lobe-like structures observed in the gamma frequencies of the electromagnetic spectrum. My project was to try to re-create these structures by simulating a particular solution to the propagation equation for cosmic rays. This partial differential equation is not usually able to be solved analytically, but we assume that there is only one single injection event from the supermassive black hole in the Milky Way about 10 million years ago. This allows for a full analytical simulation of the cosmic ray propagation given different scenarios including zero wind velocity, 1000km/s wind velocity, and a vertical 1000km/s wind velocity. The no wind and isotropic wind cases cannot create the right morphology. The Vertical wind could recreates the right morphology, though it is too bright in the center of the bubbles, which also do not extend far enough outward.

2 Introduction and Motivation

The physics of cosmic rays has been a burgeoning field as new experiments in gamma rays and synchrotron radiation have widened the exploration range of their origin, propagation, and interactions. They can enlighten much about the evolving structure of the Milky Way as they can be indicative of many different processes. This includes the phenomenon of Fermi bubbles, which are large lobes of ionized plasma in the gamma spectrum. Below, we will investigate recreating the morphology and spectra of these structures using the propagation and transport equations of cosmic rays in the Milky Way.

2.1 Cosmic Rays

Before we can discuss Fermi bubbles, we must better understand cosmic rays, which we can use to probe potential sources of Fermi bubbles. Proton-proton (pp) collisions with the baryonic gas and the cosmic rays produce the gamma rays in the galactic halo. Proton-proton (pp) collisions are much more numerous in the interstellar medium as energy losses for leptons are much greater via Coulomb interactions, Bremstrahlung, synchrotron, and inverse-Compton scattering interactions than for hadrons via ionization and Coulomb interactions. As cosmic rays propagate outwards from some injection event, they interact with the surrounding gas via these hadronuclear reactions to produce the gamma rays the telescopes see.

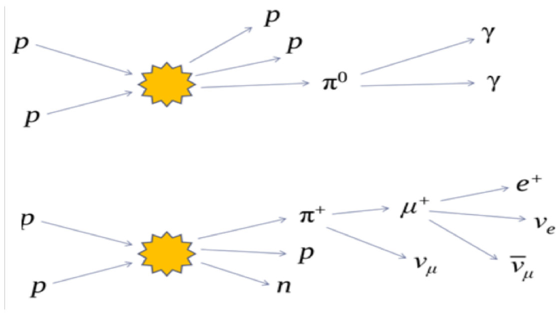

Figure 1: Depicted above is primary (top) and secondary (bottom) cosmic ray production. The cosmic ray pprotons interact with the background gas in the Galactic halo and create $\pi(0)$-decay gamma-rays and secondary electrons through proton-proton interaction.

Various phenomenological processes can create cosmic rays such as supernovae, black hole accretion, etc.

Cosmic rays usually refer to particles in a range of 1MeV and continuing to $10^{21}eV$, and can comprise of nuclei (protons to actinides), electrons, antiprotons, and positrons. They can be separated into two categories: primaries and secondaries. Primary cosmic rays are particles accelerated at astrophysical sources. Thus electrons, protons and helium, as well as carbon, oxygen, iron, and other nuclei synthesized in stars, are primaries. Secondaries are those produced by the interaction between primaries and the interstellar gas, which include nuclei such as lithium, beryllium, boron and even positrons and antiprotons. For the sake of simplicity, we will only consider primary cosmic rays by investigating the results of protons or electrons (i.e. the cosmic rays) colliding with baryonic gas and/or decaying into gamma rays, which telescopes subsequently detect. Directional information is lost for cosmic rays because the Larmour radius is on a scale much smaller than that of the Milky Way, so their resulting gamma and radio spectra are key for studying large scale distribution. Physicists can measure the number of particles for a given frequency (i.e. energy) to obtain the spectrum. Such spectra typically follow a power law, which is indicative of non-thermal processes. This power law will differ depending on the energy range of the photons. Below $5 \times 10^{15}eV$, the power law is $\frac{dN}{dE} = E^{-2.7}$. Sources of such cosmic rays are from within our own Milky Way. Beyond this energy and up to what is called the ankle (in which the spectrum returns to $\frac{dN}{dE} = E^{-2.7}$) at $3 \times 10^{18}eV$, then the spectrum follows $E^{-3.1}$. Such cosmic rays are coming from extra galactic sources. The flux is another important quantity that measures the rate of incoming photons, which measures the number of particles per area per second per steradian per energy interval [4].

2.2 Fermi Bubbles

The Fermi Long Area Telescope (Fermi LAT) released the discovery of the Fermi bubbles back in 2010. They were discovered using foreground removal techniques in which simple models of the galactic plane are created and then subtracted from the images. Though Fermi bubbles were initially observed in the gamma end of the spectrum, traces of them exist radio, microwave, X-ray, to neutrinos. For example, similar structures known as the WMAP haze (microwave) are also observed.

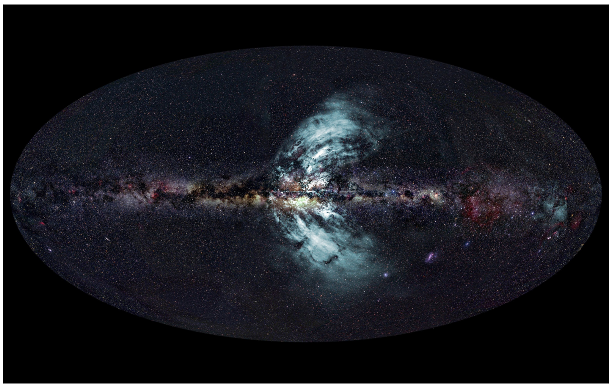

Figure 2: Pictured above is an image of the Fermi bubbles in the galactic plane. The off center features are clear.

2.2.1 Morphology of Bubbles

The bubbles are observed between the 1GeV and the 100GeV range with strong cutoff at 110GeV and a hard cosmic ray spectrum with a spectral index of -2. The two lobes extend outward about 10kpc and reach 50° above and below the galactic center. They have a width of $44circ$ in longitude. Their total gamma ray power is $10^{37}erg/s$. This gamma luminosity has a flat energy profile of the bubbles (in gamma spectrum) with a smooth surface. That is, the spectrum is spatially uniform [7].

The Fermi bubbles have similar counterparts in various energy ranges of the spectrum. For X-rays, the ROSAT all-sky survey provides images at energies .5-2keV. In [6], at 1.5keV, they observe limb brightening in X-rays along the edges of the north and south bubbles. These arc features are coincident with the edges of the gamma bubbles themselves. This is indicative of shocked gas compression existing at the edge of the bubbles, as well as a hollow "shell" structure in the X ray spectrum. This indicates a lower density inside of the bubbles.

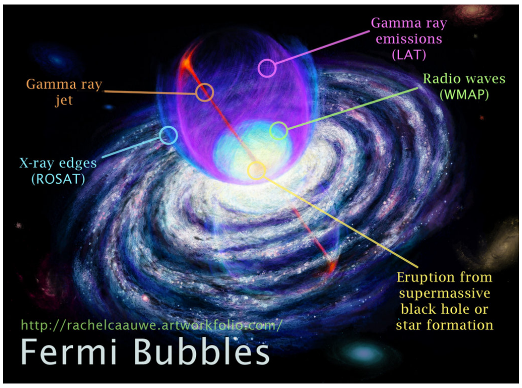

Figure 3: [5] Pictured above is an artist rendition of the Fermi bubbles as described by FermiLAT gamma emission, ROSAT x-ray emission, and WMAP microwave emission. The outer edges of the x-rays trace the gamma bubbles themselves and radially extend out further. The WMAP haze traces the gamma bubbles more precisely, but do not extend to such a larger latitude. Finally, there is a depiction of what a possible jet from a supermassive black hole might look like

For microwaves, WMAP provides microwave data, which has revealed the "microwave haze" [3]. This is a spherical structure that extend about 4kpc north and south towards the galactic center. Originally, they were predicted by models of dark matter annihilation, but the presence of shock fronts disfavors this, which is evidence of a high energy, localized injection event. Both the gamma and microwave spectra are spatially correlated and have hard spectra.

2.2.2 Potential Origins

Wind-blown bubbles with similar morphology to the Fermi bubbles also exist in other galaxies, which indicate that they may have formed during an enhanced nuclear star formation event or a Sgr A* outburst (the SMBH in the center of the Milky Way). The emission model includes a hot filled bubble components co-spatial with the gamma ray region and a shell of compressed material in the X ray. It is likely these structures were formed during some episode of energy injection roughly 10 million years ago in the galactic center. Such an event could be one of two things. The first would be accretion from the Milky Way's supermassive black hole. Such accretion episodes could produce winds or jets that inflate a cavity with thermal and nonthermal particles. The second would be from a starburst event of stellar formation that would produce an outward flowing wind. Such events could also include type II supernovae from these stars. Each type of source is capable of reaching distances of 10kpc, which is comparable to the size of the Fermi bubbles themselves.

2.3 Studying the Bubbles

Better understanding the origin of the Fermi bubbles will shed light on phenomena in the Milky Way such as cosmic rays propagation, galactic magnetic fields, and prior AGN activity. Comparing observational results with theoretical simulation has proven difficult as there is a large number of phenomena that influence the models, but cannot all be considered simultaneously. Thus, finding the right models which consider the right physics is essential. However, trying to match all of the physical observations with simulation has proven difficult, especially in simulation [1].

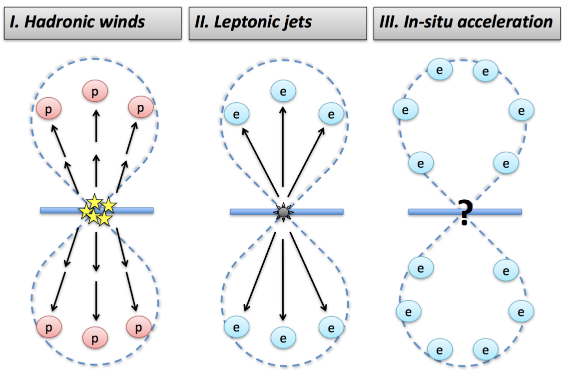

Figure 4: Pictured above are visuals of the potential mechanisms for cosmic ray transport from the galactic center. The left image are hadronuclear pp collisions from the stars emitting gas outwards. The middle image includes secondary electrons from these pp interactions, which could help recreate the microwave WMAP haze. Hadronuclear reactions cannot recreate the WMAP haze alone. The third image are a group of concentrated electron sources at the edges of the bubbles. Large reverse shocks could further supply primary cosmic rays

There are 3 different models or mechanisms for producing CRs in the Fermi bubbles: 1) hadronic pp collisions and 2) leptonic ep collisions. Hadronic reactions occur when the gamma rays are produced by inelastic collisions between protons and the thermal nuclei via decay of neutral pions. Leptonic reactions occur where the gamma rays are generated by inverse-Compton (IC) scattering of the interstellar radiation field (ISRF) by cosmic ray electrons. A pure hadronic model would extend the spectrum outward, which allows the proton spectrum to continue to high energy. Leptonic reactions would have IC scattering of a softer photon and transfer energy to those photons. If the photon is too energetic, and if it exceeds KN regime, the cross section of the leptons go down. If there are fewer collisions and would cause the spectrum to drop faster Thus, we would expect a drop in cosmic ray density for high energy. Some recent models have said that some data partially disagrees with a pure hadronic interactions. A means of cosmic rays transport includes in situ acceleration via shocks and turbulence.

3 Theory

3.1 Solving Transport Equation

When the telescopes are making measurements, they are usually measuring the spectrum (density as a function of frequency) of these photons. Below, we will derive the expression for the spectrum by solving the cosmic ray propagation equation and then manipulating the result to get the cosmic ray spectrum. This will prove useful in simulation as we can evolve the specific solution to the propagation equation to see what the resulting spectrum looks like. In this case, the specific solution refers to a single black hole injection event for cosmic rays.

We will refer you to [2] for the derivation of the drift-diffusion equation, which we use for the propagation of the cosmic rays. It is like a continuity equation, but with more terms like convection, wind, source, collisions, etc. It is used during a quasi-static state of expansion (i.e. after initial acceleration). Let's begin to paint a picture of what this equation means. n is the differential density of the cosmic rays as a function of radius, time, and energy. This is a partial differential equation that tracks the total evolution of this density as a function of energy, time, and position. As the cosmic rays will have a some source injection. They are initially accelerated and then propagate outwards. As they propagate there may be other particles in the ISM such as winds that can create mixing or other protons in which the cosmic rays collide. These ideas can be tracked using the transport equation:

$$\frac{\partial n}{\partial t} = \nabla \cdot (D_i \nabla n_i) - \frac{\partial}{\partial E}[b_i(E)n_i(E)] - \nabla \cdot u n_i(E) + Q_i(E,t) - p_i N_i + \frac{v\rho}{m}\sum_{k \geqslant i}\int \frac{d\sigma_{i,k}(E,E')}{dE} n_k(E')dE' \quad (1)$$

$n_i(E,x,t)dE'$ is the density of particles of type i at position x with energy between E and E+dE. Specifically, E refers to the energy of the cosmic rays when we detect them. We assume the wind is only a variable of the radius for simplicity. Briefly, we will ignore the last two terms. The first term from the right is a loss term via collisions or decay for the nuclei i. The latter, σ_i is the spallation cross section of the cosmic rays going a velocity v with traveling through matter with density ρ. It is a cascade term due to nuclear fragmentation processes. In this case, we will ignore such fragmentation. We will also ignore collisions and decays in this case. We will now consider the resulting equation when discussing future simulation:

$$\boxed{\frac{\partial n}{\partial t}} = \boxed{(D_i \nabla_r^2 n_i)} - \boxed{\frac{\partial}{\partial E}[b_i(E)n_i(E)]} - \boxed{\nabla_r \cdot v_w n_i(E)} + \boxed{Q_i(E,t)} \quad (2)$$

3.1.1 Time Derivative

The green term is the time evolution of the cosmic ray density.

3.1.2 Diffusion Term

The cyan term is the diffusion term in which D(E), the energy dependent diffusion coefficient relates the current of the particles to the density of the particles. Please note that we adopt a spatially and temporally independent diffusion coefficient. The larger the diffusion coefficient, the more the particles flow outward away from the source.

$$J(r,t) = -D\nabla n \quad (3)$$

The diffusion coefficient has units of $length^2 \times time^{-1}$. This term may look familiar if we recall from the simple continuity equation that.

$$\dot{n}(r,t) \propto -\nabla J(r,t)) \quad (4)$$

As the particles flow out of some region, they are decreasing in number over time. Equation 3 can be substituted into equation 4 to obtain the second term of equation 2 ($D_i \nabla_r^2 n_i$). Note that we treat D as spatially and temporally independent so this term will look like a Laplacian of the cosmic ray density. Physically interpreted, this looks like a mixing term as the Laplacian is a measure of how the gradient diverges. In other words, for a larger D(E), the particles will diverge faster from their original flow, and thus diffuse more quickly. Thus, the value of D(E) is essential to properly measure how the particles are flowing. Calculating the Diffusion coefficient is highly non-trivial as it entails two factors: 1) external turbulence and 2) scattering from magnetohydrodynamics.

$$D = \frac{\langle v \rangle \cdot l_{mfp}(E)}{3} = \frac{c l_{mfp}(E)}{3} \tag{5}$$

The photons are traveling at a velocity c, and l_{mfp} is the mean free path of the cosmic rays, which is typically the distance in which a particle has traveled before drastically changing trajectory. This component of the diffusion constant in equation 5 arises from perturbation of the halo medium (e.g. outflows). The large scale magnetic field will then cascade down to small scale, which results in turbulence. The other more complicated component to the diffusion coefficient is due to the streaming instability of cosmic ray themselves. Because cosmic rays are charged particles, when they propagate, they can drive magneto-hydrodynamic waves. These waves then scatter the cosmic rays outward. This creates a more dynamic diffusion coefficient.

CR's could also evolved down their pressure gradient via scattering from self-excited Alfen waves (oscillations in plasma due to interactions between plasma and oscillation magnetic fields). However, the slow growth rate of Alfven waves makes the effect of CR instability negligible.

3.1.3 Energy Loss

The blue term is an energy loss and gain term in which tracks how expansion and collisions result in energy loss

$$b_i(E) \equiv -\frac{dE}{dt} = (\kappa \sigma_{pp}(E) \bar{n}(r) c E + (v_w/r))E \tag{6}$$

This loss term can represent acceleration or energy loss processes such as ionization. The κ is the inelasticity of the pp collision with a cross section σ_{pp} for particles with an energy E and a gas density profile $\bar{n}(r)$. In the second term, the wind velocity causes an adiabatic expansion and thus some cooling. Since the gas density in the halo is $\approx 10^{-3} - 10^{-5} cm^{-3}$. This means that for each interaction, a proton loses $.17 * \sigma_{pp} * n_g c$. n_g is the gas density profile along the line of sight. However, in this case, we will be ignoring the energy loss term due to collisions because in this case adiabatic cooling due to the expanding wind will dominate. Thus, $b_i(E)$ is simply $(v_w/r)E$.

3.1.4 Convection

Since the The violet term is a convection term with velocity v_w. It tracks the large scale convection of the cosmic rays, which could have multiple sources. In this case, v_w is the wind velocity, and assumed to be radially constant. This term entails movement of the particles due to pressure gradients due to a large scale wind which could be launched by various mechanisms.

3.1.5 Source

The last red term is probably the most important for the sake of this project because it is the injection source term of the cosmic rays. The geometry, time evolution, and energy dependence of the source is reflected in this term. In this case,

$$(E,t) = S(t)Q_o(E) = \delta(t - t_o)S(t_o)Q_o(E) \tag{7}$$

at time tm where S(t) describes the CR injection history. Because we are investigating the injection of cosmic rays via the SMBH SgrA* in the Milky Way, then we assume a S(t) is delta function in time dependence. This is because on the time scale of 10Myr, an expected injection time of $\approx$ 30,000years, is sufficiently short injection relative to the evolution itself that we can treat it as a point injection. For the energy dependence, we can adopt $Q_o(E) = N_0(E/1GeV)^{-p}$ as the injection rate for today. This is

To see how we solve this equation for the density of the cosmic rays, see the appendix. From here we will work with the resulting solution for the density of the cosmic rays from some source of radius r_g:

$$n(t,r,E,r_g) = \frac{\pi^{3/2}}{(2\pi)^3}\left[\int_{t_g}^{t} dt' Q(\mathcal{E}',t') \times \frac{exp[-(r-r_g-s)^2/4\lambda(E,t')]}{\lambda(E,t')^{3/2}}\right] \times exp\left[\int_{t}^{t} dt" \frac{\partial b(\mathcal{E}'',t)}{\partial \mathcal{E}"}\right] \tag{8}$$

where $s = \int_{t'}^{t} v dt"$ and $\lambda(E,t') = \int_{t'}^{t} D(\mathcal{E}")dt"$. In this case, $\mathcal{E}"$ means the energy of the CR at time t" or t', which has energy E at present time. This solution is for the CR density from a source at r_g, which in this case is the supermassive black hole at the center of the Milky Way. This will allow for a much simpler analytical solution to equation 3. Without wind, the number of cosmic rays would be expected to monotonically decrease outward radially as is reminiscent of the leaky box model of cosmic rays. With a wind, the overall density would be lower as the wind carries the cosmic rays out of the Milky Way and into the intergalactic medium. This curve would be a concave down curve as the number of cosmic rays increase radially as they are quickly carried out of the center of the galaxy and peaking at some intermediate radius away. Then the density would begin to decrease again.

3.2 Obtaining the Spectrum

Upon calculating the CR distribution and the gas distribution in the halo, we can calculate the gamma-ray emissivity $J_\gamma(E_\gamma, r)$ $(GeV cm^{-3} s^{-1})$ at a specific distance r, which is a measure of how the rate of energy traveling through a volume in space is denoted by

$$J_\gamma(E_\gamma, r) \equiv \frac{dN_\gamma}{dE_\gamma dt} = cn_g(r)\int_{E_\gamma}^{\infty} \sigma_{pp} N(r,E) F_\gamma(\frac{E_\gamma}{E}, E)\frac{dE}{E} \tag{9}$$

where F_γ is the spectrum of the secondary gamma-rays in a single collision. Thus we must integrate over the spectrum in order to obtain this emissivity expression. The total gamma ray flux then is the emissivity evolved over a distance and averaged over the solid angle at Earth:

$$\Phi_\gamma(E_\gamma) = \frac{1}{\Omega_{FB}}\frac{J_\gamma(E_\gamma,0)}{4\pi r_E^2} \tag{10}$$

$$\times\left[1 - \theta(1kpc - |z|)\right] \times \theta\left(sin^{-1}\frac{|z|}{|r - r_E|} - 10\circ\right)$$

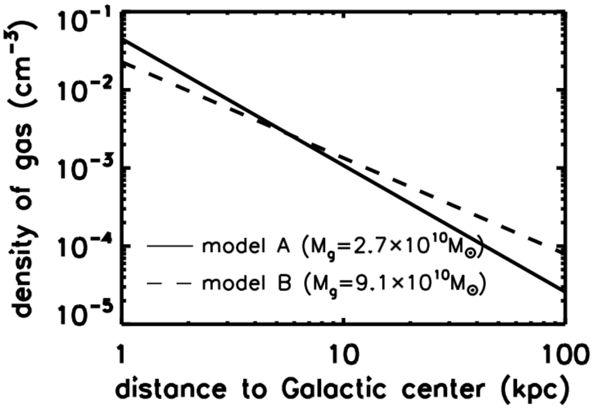

Figure 5: Pictured above is the function $n_g(r)$, which is the gas density profile as a function of the radius. We can see that it has a constant slope and slowly decreases.

where $\theta(x)$ is the Heavyside function and r_E is the radius to the Earth from the galactic center. This will be the equation we use to calculate the flux when tracking the evolution of the cosmic rays over time. It contains the familiar inverse square law to allow for particles to propagate outwards (towards Earth). The second step function allows us to only consider a galactic latitude $|b < 10\circ|$, which is consistent with the FermiLAT analysis of the Fermi bubbles [6]. We determined Ω_{FB} that corresponds to the region where the intensity is greater than 10^{-7}.

4 Methods

Throughout this project we used Fortran, python and C code to code equation 3 into in order to move the solution for the cosmic ray density forward in time after a single injection. The output of this code was a series of cosmic ray density files at different energies, radii, and angles. Once this code ran, then the resulting CR density files would be put into a piece of code that would calculate the spectrum of the cosmic rays.

4.1 Implementing the Solution

Upon having this solution, we needed to be able to take all of the important variables in equation , in order to simulate the evolution of the cosmic ray density. First, we assumed that there is a single cosmic ray injection point about 10 million years ago at the center of the galaxy by the supermassive black hole. After this point, the cosmic rays are no longer being accelerated. This significantly simplifies the computation when running the code for two reasons: 1) considering a point injection means we do not need to loop over two spatial coordinates (i.e. if the injection source spanned some area) and 2) it simplifies the integration from two time integration to one time integration. This would mean that the form of the time dependent piece of the source term is a single delta function $\delta(t - t_o)$. This means that

$$Q(E, t) = \delta(t - t_o)S(t_o)Q_o(E)$$

. Thus, the form of equation 3 will select out all values of the integrands at injection time t_o:

$$n(t,r,E,r_g) = \frac{\pi^{3/2}}{(2\pi)^3}\Big[Q(\mathcal{E}',t_o) \times \frac{exp[-(r-s)^2/4\lambda(E,t_o)]}{\lambda(E,t_o)^{3/2}} \times exp[\int_{t_o}^{t} dt" \frac{\partial b(\mathcal{E}'',t)}{\partial \mathcal{E}"}]\Big] \tag{11}$$

where recall $\lambda(E,t_o) = \int_{t_o}^{t} D(\mathcal{E}")dt"$ is the time integral of the diffusion coefficient. In this case we adopt an injection time of $t - t_o \approx 30,000$years. This is a sufficiently small time scale that the delta function approximation for the source is still valid. It also is on the same order of time in which a supermassive black hole could be accreting and ejecting material outward.

4.2 Parameter Choices

However, we still do not have all of the information. In order to do calculations, we need to pinpoint physical values for the parameters in the code.

4.2.1 Diffusion Coefficient

The diffusion coefficient values we adopt are spatially and temprally independent. They are calculated from simulation considering turbulence and magnetohydrodynamics.

Diffusion of the cosmic rays outward from the center of the galaxy can be extremely complex as the cosmic rays are often charged particles interacting with the surrounding ISM. This physically means that turbulence and magnetohydrodynamics become relevant and make the calculations of the diffusion coefficient become much more complicated. We can then integrate these values to obtain the λ term in equation 11.

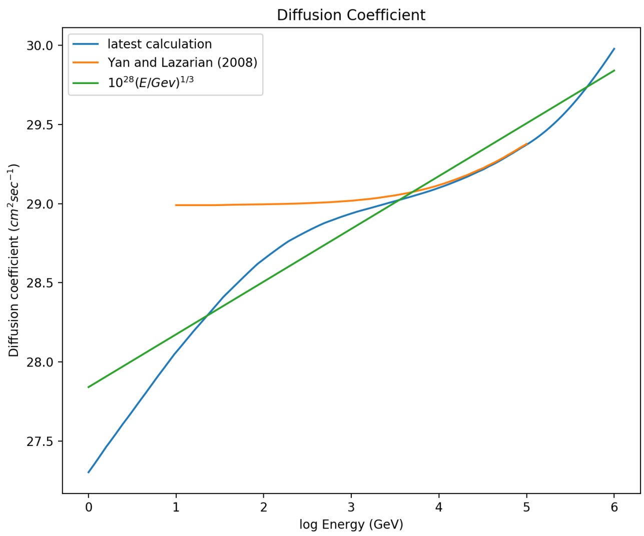

Figure 6: Pictured above are a few different models for the diffusion coefficient. The green curve is a common simple model for diffusion in the galactic disk. The orange curve considers turbulence alone of the particles, which increases mixing for higher energy particles. The blue curve also includes magnetohydrodynamics, which introduces some inflection points that reflect how magnetic fields can reduce mixing for lower energy particles where the fields dominate. In order words, when the diffusion coefficient is small, the cosmic rays do not have enough energy to escape the wind, resulting in large adiabatic losses.

4.2.2 Injected Power

We need to know what $S(t_o)Q_o(E)$ look like as a quantity. Recall, the energy dependence of cosmic rays follow a power law, such that the energy dependent term is $Q(E) = N_o(\frac{E}{1GeV})^{-\alpha} \propto \frac{dN}{dE}$. This is the injection rate today, so the full time dependent source term will look like

$$Q(E,t) = \delta(t-t_o)S(t_o)Q_o(E) \tag{12}$$
$$= \delta(t-t_o)S(t_o)N_o(\frac{E}{1GeV})^{-\alpha}$$

α here will be 2.2. E will be the range of cosmic ray energies we are considering, which in this case will be from .1GeV to 1000GeV. $S(t_o)$ is usually a time evolving piece, but in this case is just 1 to consider the single time injection rather than a time evolving, continuous piece. N_o is a multiplicative normalization constant, which depends on the total luminosity of the cosmic rays. We can solve for N_o by integrating Q(E) over the energy range to to get the total luminosity L_{CR}

$$\int_{1GeV}^{\infty} EQ_o(E)dE = L_{CR,0}$$

$$\int_{1GeV}^{\infty} EN_o(\frac{E}{1GeV})^{-\alpha}dE = L_{CR,0}$$

We can define the injected power in the code as needed, so in order to have a value for equation 12, we can solve for N_o given some initial injected Luminosity. This can vary from $10^{41} - 10^{43} ergs$. The upper limit in this case corresponds to the Eddington luminosity, which is the maximal ejected power that a black hole can emit. Thus the final value for the normalization factor is:

$$N_o = \frac{L_{CR,0}(2-\alpha)}{E^{2-\alpha}} \tag{13}$$

4.2.3 Wind Speed

There is a wide range of uncertainty for the wind speed of the bubbles ranging from slow ($\approx$ few hundred) to fast (>1000km/s) outflows from the galactic center. However, if the speed is too low, the gas will not propagate far enough to recreate the bubbles themselves. This value will manifest in the collision term of equation 11 because $b = (v_w/r)E$.

5 Results

We consider various quantities when plotting the results: 1) the cosmic ray density as a function of radius, 2) the sky map of the cosmic ray density, and 3) the resulting spectrum for different cases.

When considering how well the results recreate the Fermi bubbles, we need to consider two things 1) the morphology of the cosmic rays in the skymaps and 2) the shape of the flux curves The gif skymaps have a higher resolution as the flux is calculated for each pixel, rather than for the whole bubble. For the flux plots, as the bubbles grow, the solid angle is increasing, which would cause the flux to decrease. This means that the magnitude of the flux curves can mean very little if the morphology is incorrect. For example, if the bubbles are faint over a small area, then they may match the spectra of brighter, larger bubbles. When considering the flux curves, the shape relative to the data in this case is much more important.

As the wind expands, the cosmic rays are carried away from us to regions of lower density. We need flux above 10^{55} ergs injected into the bubble region in order to have the proper amount of radiation.

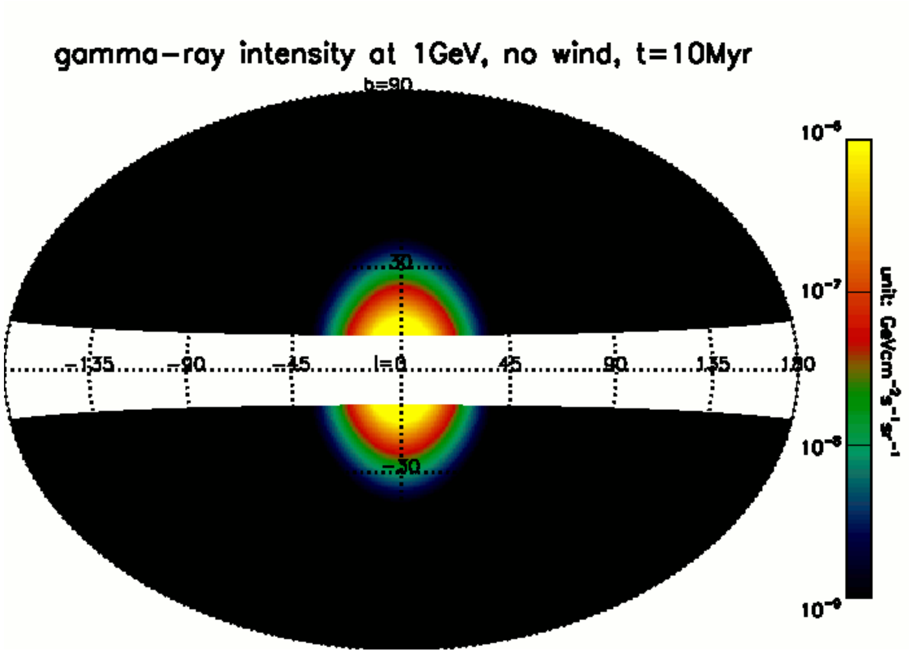

Figure 7: Above pictured is the morphology of the cosmic rays after 10Myr in which there is pure diffusion and no wind. The intensity is still too bright at the center and the bubble is much too small

This is because the injection time and the injection energy rate are assumed to be constant, and their product is L_{CR}∗time $= 10^{55}$ergs. The flux can be consistent which this, but the morphology is not. In theory, this could last over a longer period of time, which would mean that the total luminosity does not technically need to be 10^{55}ergs.

6 Discussion

6.0.1 No Wind Case

When there is no wind, the cosmic rays only diffuse and slowly expand outwards. If the wind velocity is too low, the bubbles would take too long to form. At low energy, the diffusion coefficient is smaller, so the cosmic rays do not diffuse outward as quickly. The morphology of the radial wind is not consistent with what we would expect of the Fermi Bubbles. Because now we only count the emission above 10 degrees and those outside of the disk, the spectra for the no wind case still drops very quickly. At lower energies over time, the particles diffuse out to higher latitudes so there are more low energy particles.

6.0.2 Radial Wind Case

An isotropic wind fills the sky with too many cosmic rays . The flux of these bubbles is too high by an order of magnitude and begins to fill the entire sky rather than produce a bubble-like structure. This is because horizontal components, i.e. parallel to the galactic plane, carry too many cosmic rays towards the Earth and result in a much larger flux.

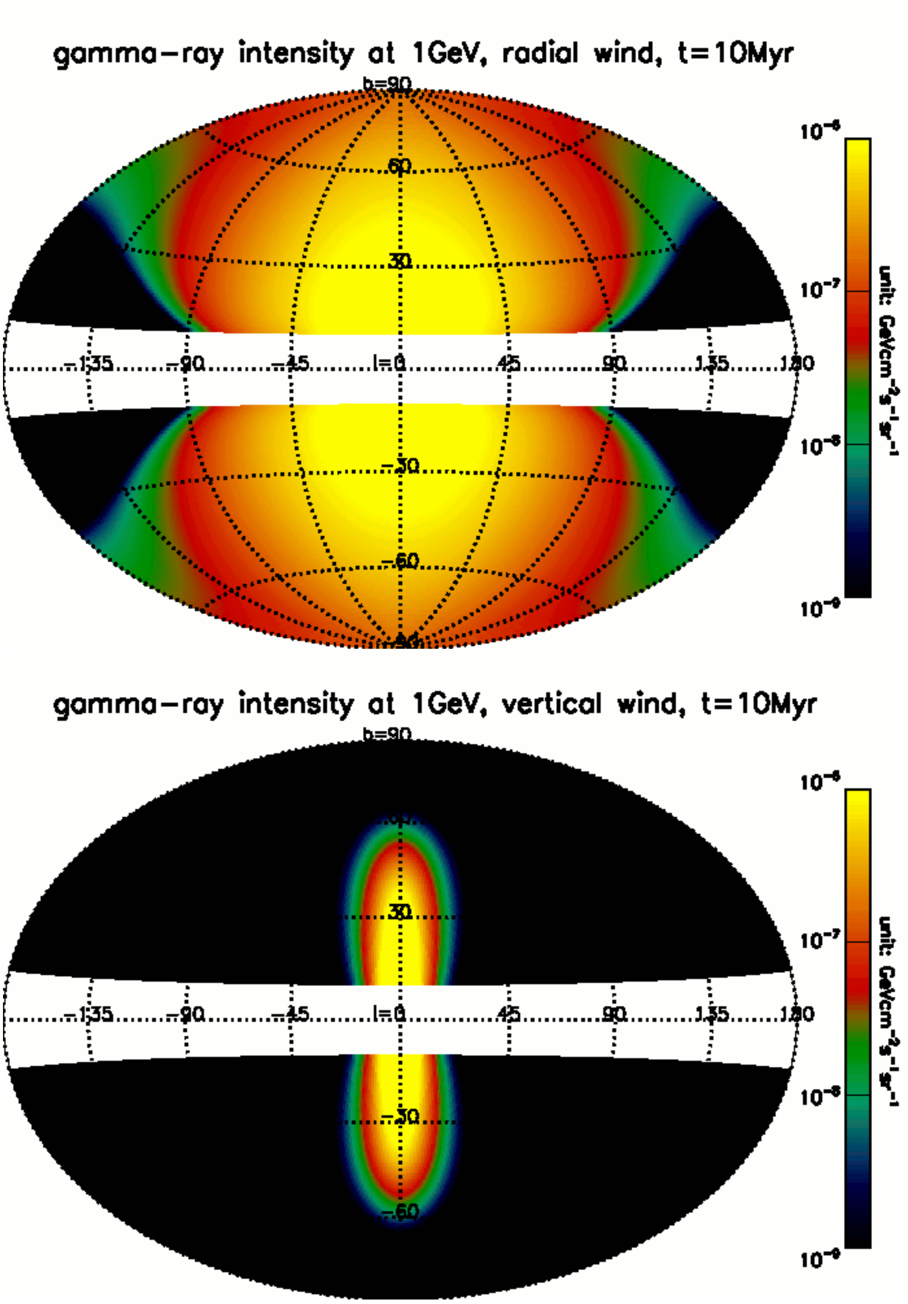

Figure 8: Above pictured is the morphology of the cosmic rays after 10Myr with am isotropic wind in all directions. The cosmic rays overwhelm the whole sky and are much too bright by over an order of magnitude. There is no clear bubble morphology, which id indicative of too many cosmic rays propagating outwards in all directions. A vertical wind is possible, but the speed is more important. The regular high speed wind creates a problem for the spectrum because it brings too many cosmic rays to the Earth. We need some more vertical components because otherwise too much wind is sent to the Earth.

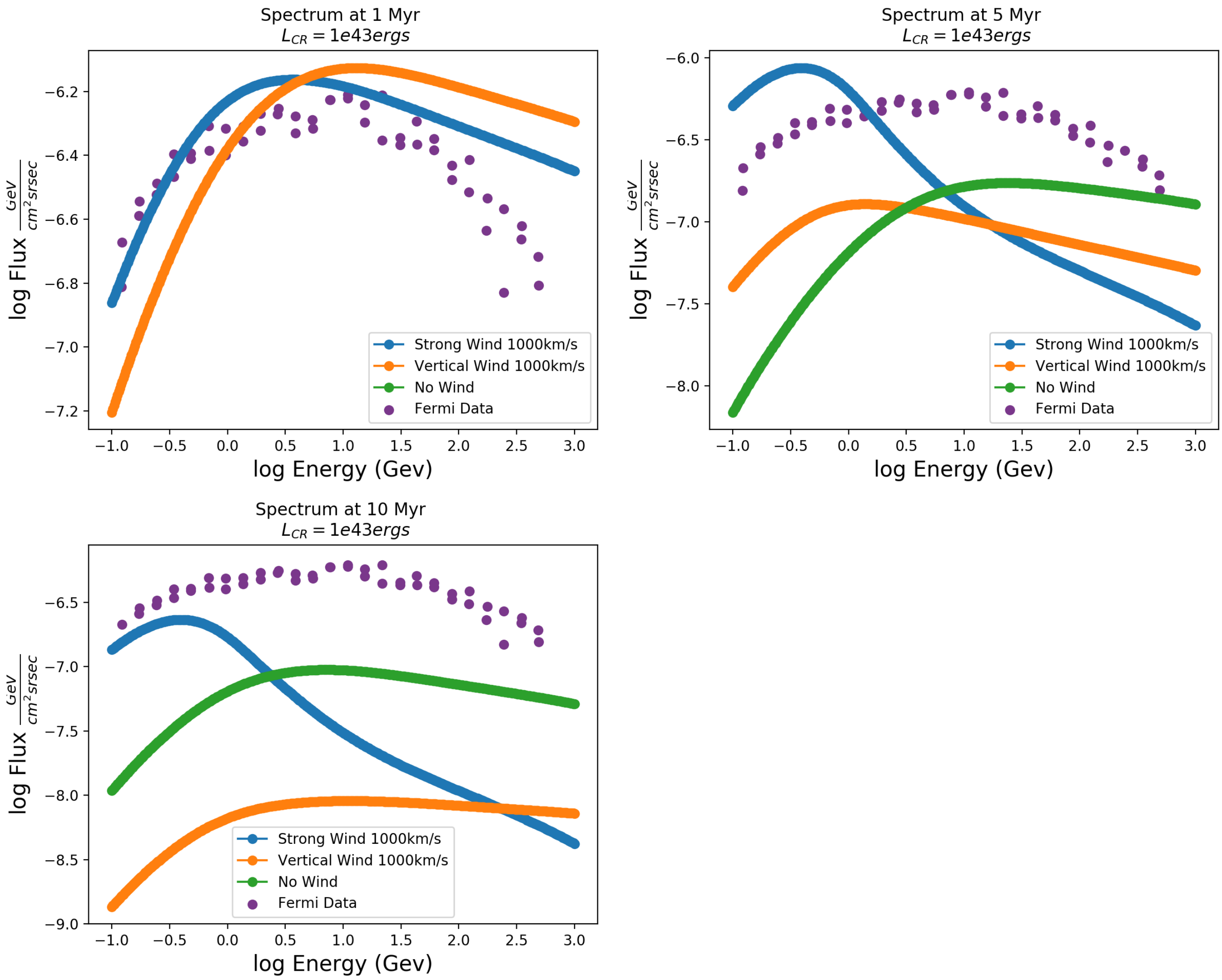

Figure 9: After 1Myr, the no wind case does not appear above because the solid angle subtended by the bubble is near zero. This means there is essentially no flux from the cosmic rays at this time. The case with vertical wind will have more high energy particles escaping than the low wind case. The lower energy particles will . Above we can see the evolution of the spectra after five million years. There is a large jump in low energy cosmic rays in the strong wind case. This could be because the high energy cosmic rays travel outward too far, in which they would look fainter because of the inverse square relationship between flux and distance. Thus, particles that propagate out farther will appear fainter. This explains the overall drop in magnitude between 5Myr and 10Myr as all of the particles eventually propagate outward. The shape of the curve changes less between these two figures. For these graphs, the magnitude of the curves is less important because these can be simply influenced by other factors such as the injection energy from the black hole. However, the shape is much more important. Here, we see the shape of the strong vertical wind and the no wind case each similarly match that of the data. This is slightly misleading, because the morphology of the no wind case poorly matches that of the Fermi bubbles themselves. The strong vertical wind has a flatter flux profile, which is what we expect from observation.

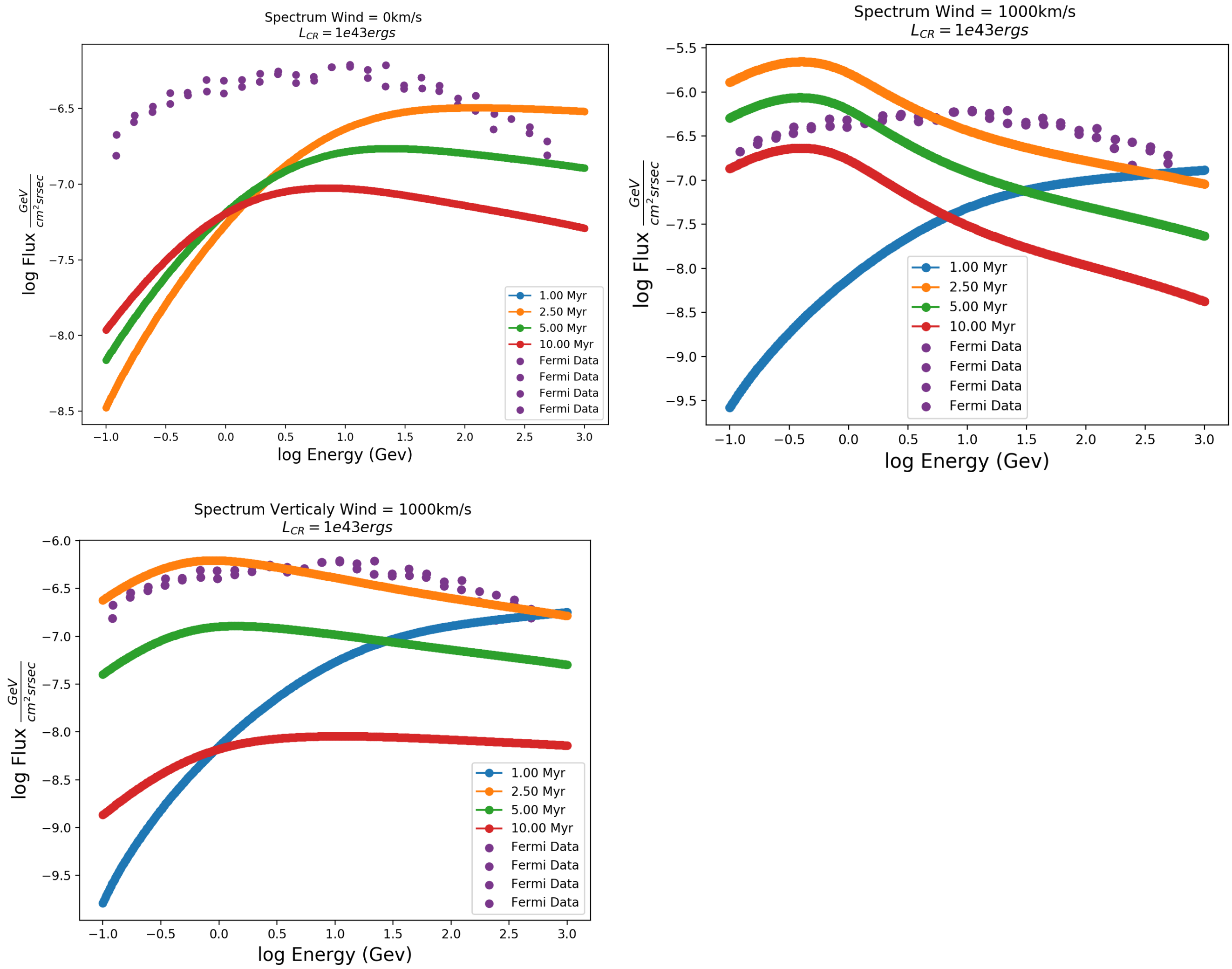

Figure 10: pictured above is a similar set of plots as figure 9, but here the individual plots are separated by the conditions of the wind rather than by time. For the no wind case (top left), we can see that the low energy particles slowly propagate outward over time and the high energy particles slowly dim as expected. For the isotropic wind case, this occurs on a much faster time scale in which the low energy particles travel outward on a rapid timescale and then slowly the flux decreases as the particles are traveling further away from the Earth. This effect is more prominant for the vertical wind case (botton left) as the injected particles are traveling away from the Earth more quickly than those with an isotropic velocity. It is clear that the vertical wind case matches the shape of the Fermi data the best. The only problem is that of time scale and how rapid the particles are expanding outward. Future work may tweak the parameters that will influence the overall magnitude of the flux without changing the shape too much.

6.0.3 Vertical Wind Case

In the vertical wind case , at 10Myr, the flux decreases because the wind is carries them perpendicular to the galactic plane. This means the cosmic rays will travel to a much farther region. Now the cosmic rays are interacting with low density regions that are also farther from us. As they travel outward, they also will look fainter because they are farther away.

The vertical wind gives the best case for these scenarios because it creates a similar morphology to the Fermi bubbles, and a spectrum with a similar shape. Though the bubbles for the vertical case are still too small to accurately represent the Fermi bubbles and only extend to about $\approx$ 7-8kpc rather than the expected 10kpc.

6.1 Moving Forward

Moving forward, our investigation can include a number of things, which fall into two main categories: 1) parameter tweaking in the initial model to decrease inner flux and create larger bubbles and 2) try to also recreate corresponding morphologies in microwave/xrays.

Changing the parameters is a very easy change to make because now we know some kind of properties that will create the bubbles we want.

- introduce a flat gas density profile to lower the flux for the inner radii
- We can increase the injection spectral index, which would mean the spectrum has a steep slope, so there are fewer high energy particles. This will help mitigate anywhere there is too much power.
- Introduce wind with some opening solid angle
- Try to also recreate morphologies in microwave/xray
- Introduce the secondary leptonic interactions because pure hadronic processes cannot recreate similar structures seen in xrays and microwaves

6.1.1 Gas Density Profile

The center of the bubbles in the maps is still too bright. This could be fixed by changing the gas density profile that the cosmic rays interact with while radiating outwards. The particles are traveling into a region where the gas density is lower, so the emission is lower as they expand outward. The gas density profile still has a high uncertainty. Because of this, moving forward, we could adopt a flatter profile for the gas density. Rather than a gas profile with a negative slope, adopting one with a near zero slope will mean that the number of interactions for the inner radii will decrease and those in the outer radii to increase. This means that the center of the bubbles may not be too bright in subsequent simulations.

Simulations are showing the gas density is very low in the bubble , which means the pp interactions are not efficient. Full MHD simulation finds that the density of the gas is very small, which means that the pp interactions are low (there is less gas) This is simulation, which has a lot of uncertainty. When they use the beta model - the gas density profile we adopt - they find this is consistent with the gas density in the halo. This may not extend to the very center of the galaxy when the radii are very low. Our assumption for the gas density profile may not be correct, but we do not have observation that disagrees with it. There is no alternative for now.

6.1.2 Leptonic Extensions

A pure hadronic model would extend the spectrum outward, causes the proton spectrum to continue to high energy. Leptonic reactions would have IC scattering of a softer photon and transfer energy to the photon. If the photon is too energetic, and if it exceeds KN regime (an energy regime in which the cross section goes down), then the number of collisions drop significantly and the spectrum will subsequently drop.

Some recent models have said that some data disagrees with pure hadronic interactions, so moving forward, it would be wise to also include leptonic interactions somewhere in the code. If a secondary process is included within the algorithm, then a final spectrum can be used to explain the drop in high energy particles.

6.1.3 Concluding statements

This project investigated the hadronic origins of the Fermi bubbles by using simulation.

The discovery of the Fermi bubbles in the Milky Way opened up a new exploration of understanding cosmic ray processes and structures in the Milky Way itself. Their precise origins, be it AGN-like activity from SMBH SGR *A or a starburst of nuclear stellar activity, are still unknown, and much research today being done is investigating the viability of either source-type. Moreover, these sources create cosmic rays which can be hadronic (i.e. proton collisions producing gammas) or leptonic (i.e. proton collisions resulting in electrons). The former is higher energy and creates the gamma Fermi bubble structure, but the latter is necessary to produce the corresponding structures in other regions of the electromagnetic end of the spectrum.

In addition to data, a major way researchers do this is through simulation. Simulating these processes and subsequent structures can prove extremely difficult and computationally expensive. However, simplifications in the differential equations made using the point source model allows for effective investigation of hadronic origins for these Fermi bubbles.

This project used a specific solution of the cosmic ray transport equation to simulate the transport of the cosmic rays given a single black hole injection event roughly 10Myr ago. We simulated given different scenarios including zero wind velocity, 1000km/s wind velocity, and a vertical 1000km/s wind velocity. The no wind and isotropic wind cases cannot create the right morphology. The Vertical wind could recreates the right morphology, though it is too bright in the center of the bubbles, which also do not extend far enough outward.

Appendices

A Deriving Cosmic Ray Density

From here let's work through the derivation to obtain the solution of the cosmic ray density as a function of radius, time, and energy. Let's begin with a slightly rearranged form of equation 2. For now, we will ignore the convection term

$$\frac{\partial n}{\partial t} + \nabla \cdot u n_i(E) + D_i(E)\nabla^2 n_i - \frac{\partial}{\partial E}[b_i(E)n_i(E)] = Q_i(E,t)\delta^3(r - r_g) \tag{14}$$

In order to be able to solve this equation we must use the definition of the Fourier transform and the delta function

$$n = \frac{1}{2\pi^3}\int d\omega f_\omega e^{iwx}$$

$$\delta^3(x) = \frac{1}{2\pi^3}\int d\omega e^{iwx}$$

We can turn use these to turn equation 3 into the following

$$\frac{\partial f_\omega}{\partial t} + \omega u f_\omega + (\omega^2 D(E) - \frac{\partial b}{\partial E})f_\omega - b_i(E)\frac{\partial}{\partial E}f_\omega = Q(E,t) \tag{15}$$

we can define a coordinate transformation with a new set of variavles in order to turn this PDE into an ODE, which then makes it solvable. We must define the variables

$$\xi = \xi(t,E)\eta = \eta(t,E)$$

so we can now have

$$\frac{\partial f_\omega}{\partial t} = \frac{f_\omega}{\partial \xi}\frac{\partial \xi}{\partial t} + \frac{\partial f_\omega}{\partial \eta}\frac{\partial \eta}{\partial t}$$

$$\frac{\partial f_\omega}{\partial E} = \frac{f_\omega}{\partial \xi}\frac{\partial \xi}{\partial E} + \frac{\partial f_\omega}{\partial \eta}\frac{\partial \eta}{\partial E}$$

upon substituting into the equation 4 to obtain

$$\left(\frac{\partial \xi}{\partial t} - b(E,t)\frac{\partial \xi}{\partial E}\right)\frac{\partial f_\omega}{\partial \xi} + \left(\frac{\partial \eta}{\partial t} - b(E,t)\frac{\partial \eta}{\partial E}\right)\frac{\partial f_\omega}{\partial \eta} + \left(\omega^2 D - \frac{\partial b(E,t)}{\partial E}\right)f_\omega - \omega v f_\omega = Q(E,t)$$

we can choose $\eta(t,E)$ to make a quantity in the parentheses zero, that is $\frac{\partial \eta}{\partial t} - b(E,t)\frac{\partial \eta}{\partial E} = 0$. In order for this to be true, it is clear that dE/dt = -b(E,t). Thus, the above condition allows us to recognize the definition of the differential of $d\eta$ which is $\frac{\partial \eta}{\partial t}dt + \frac{\partial \eta}{\partial E}dE = \partial \eta = 0$. This is the same as the constant η curve in the (t,E) plane. Thus we can solve the equation dE/dt = -b(E,t) to get:

$$\int \frac{dE}{b(E)} + t = k$$

where k is an arbitrary constant and we choose $\eta(t,E) = k = \int \frac{dE}{b(E)} + t$. We also choose $\xi = t$ out of convenience. Thus, the equation becomes:

$$\frac{\partial f\omega}{\partial t} + \left(\omega^2 D - \omega v - \frac{\partial b(E,t}{\partial E}\right)f_\omega = Q(E,t)$$

The result of solving this ordinary differential equation is

$$f_\omega = \int_{t_g}^{t} dt' Q(\mathcal{E}', t') \times exp\left[\int_{t'}^{t} (\omega^2 D - \omega v - \frac{\partial b(E,t}{\partial E}) dt"\right] \times Cexp\left[\int_{0}^{t} dt' (\omega^2 D - \omega v - \frac{\partial b(E,t'}{\partial E})\right] \quad (16)$$

where C is a constant of integration. Now we introduce the notation that $\lambda = \int_{t'}^{t} Ddt"$. If the energy loss rate and diffusion constant are temporally independent, and only functions of energy, then we can also rewrite $\lambda(E,t') = \int^{E_g} E \frac{D(E')}{b(E')} dE'$. To obtain a final expression for the CR density n(t,E) instead of f_ω, we can use some tricks with completing the square:

$$i\omega x - \omega^2 \lambda = -\lambda\big(\omega - i\frac{x}{2\lambda}\big)^2 - \frac{x^2}{4\lambda}$$

where in this case, $x^2 = r^2 - r_g^2 - s^2$ and $s = \int v dt$. Using these identities, we can arrive at,

$$n(t,r,E,r_g) = \frac{\pi^{3/2}}{(2\pi)^3}\left[\int_{t_g}^{t} dt' Q(\mathcal{E}',t') \times \frac{exp[-(r - r_g - s)^2/4\lambda(E,t')]}{\lambda(E,t')^{3/2}}\right] \times exp\left[\int_{t}^{t} dt" \frac{\partial b(\mathcal{E}'',t)}{\partial \mathcal{E}"}\right] \times exp\left[\int_{t}^{t} dt" \frac{\partial b(\mathcal{E}'',t)}{\partial \mathcal{E}"}\right]$$
$$+ \frac{C}{\pi^{3/2}} \frac{exp[-(r - r_g - s)^2/4\lambda(E,t')]}{\lambda(E,0)^{3/2}}\Bigg] \times exp\left[\int_{0}^{t} dt" \frac{\partial b(\mathcal{E}'',t)}{\partial \mathcal{E}"}\right] \quad (17)$$

E′ and E′′ are the energies of a particle, whose energy is E at the present time, at t′ and t′′ respectively. For a homogeneous distribution of D at the entire space, we do not expect n to depend on a non-injection related component. Thus, we take C = 0 and the solution becomes

References

[1] M. Ackermann, A. Albert, W. B. Atwood, L. Baldini, J. Ballet, G. Barbiellini, D. Bastieri, R. Bellazzini, E. Bissaldi, R. D. Blandford, E. D. Bloom, E. Bottacini, T. J. Brandt, J. Bregeon, P. Bruel, R. Buehler, S. Buson, G. A. Caliandro, R. A. Cameron, M. Caragiulo, P. A. Caraveo, E. Cavazzuti, C. Cecchi, E. Charles, A. Chekhtman, J. Chiang, G. Chiaro, S. Ciprini, R. Claus, J. Cohen-Tanugi, J. Conrad, S. Cutini, F. D'Ammando, A. de Angelis, F. de Palma, C. D. Dermer, S. W. Digel, L. Di Venere, E. d. C. e. Silva, P. S. Drell, C. Favuzzi, E. C. Ferrara, W. B. Focke, A. Franckowiak, Y. Fukazawa, S. Funk, P. Fusco, F. Gargano, D. Gasparrini, S. Germani, N. Giglietto, F. Giordano, M. Giroletti, G. Godfrey, G. A. Gomez-Vargas, I. A. Grenier, S. Guiriec, D. Hadasch, A. K. Harding, E. Hays, J. W. Hewitt, X. Hou, T. Jogler, G. Jóhannesson, A. S. Johnson, W. N. Johnson, T. Kamae, J. Kataoka, J. Knödlseder, D. Kocevski, M. Kuss, S. Larsson, L. Latronico, F. Longo, F. Loparco, M. N. Lovellette, P. Lubrano, D. Malyshev, A. Manfreda, F. Massaro, M. Mayer, M. N. Mazziotta, J. E. McEnery, P. F. Michelson, W. Mitthumsiri, T. Mizuno, M. E. Monzani, A. Morselli, I. V. Moskalenko, S. Murgia, R. Nemmen, E. Nuss, T. Ohsugi, N. Omodei, M. Orienti, E. Orlando, J. F. Ormes, D. Paneque, J. H. Panetta, J. S. Perkins, M. Pesce-Rollins, V. Petrosian, F. Piron, G. Pivato, S. Rainò, R. Rando, M. Razzano, S. Razzaque, A. Reimer, O. Reimer, M. Sánchez-Conde, M. Schaal, A. Schulz, C. Sgrò, E. J. Siskind, G. Spandre, P. Spinelli, Ł. Stawarz, A. W. Strong, D. J. Suson, M. Tahara, H. Takahashi, J. B. Thayer, L. Tibaldo, M. Tinivella, D. F. Torres, G. Tosti, E. Troja, Y. Uchiyama, G. Vianello, M. Werner, B. L. Winer, K. S. Wood, M. Wood, and G. Zaharijas. The Spectrum and Morphology of the Fermi Bubbles, September 2014.

[2] V. Berezinsky and A. Z. Gazizov. Diffusion of Cosmic Rays in the Expanding Universe. I., May 2006.

[3] Douglas P. Finkbeiner. Microwave interstellar medium emission observed by the wilkinson microwave anisotropy probe, 2004.

[4] I. A. Grenier, J. H. Black, and A. W. Strong. The Nine Lives of Cosmic Rays in Galaxies, August 2015.

[5] Caauwe Rachel, 2018.

[6] M. Su, T. R. Slatyer, and D. P. Finkbeiner. Giant Gamma-ray Bubbles from Fermi-LAT: Active Galactic Nucleus Activity or Bipolar Galactic Wind?, December 2010.

[7] H.-Y. Karen Yang, Mateusz Ruszkowski, and Ellen G. Zweibel. Unveiling the origin of the fermi bubbles, 2018.